

# Distant clock synchronization using entangled photon pairs

Alejandra Valencia, Giuliano Scarcelli and Yanhua Shih

*Department of Physics, University of Maryland, Baltimore County,*

*Baltimore, Maryland 21250*

## Abstract

We report a proof-of-principle experiment on distant clock synchronization. Besides the achievement of picosecond resolution at 3 kilometer distance, this experiment demonstrated a novel concept for high accuracy non-local timing and positioning based on the quantum feature of entangled states.

Accurate timing and positioning metrological measurements are important for both fundamental research and practical applications. In particular, distant clock synchronization has attracted a great deal of attention in recent years due to its essential role in the Global Positioning System (GPS) and telecommunications [1].

Modern clocks have been improved to such a level [2], that the resolution and accuracy of the comparison techniques have become the limiting factors to determine their relative rates and synchronization. There are two standard methods for synchronizing two distant clocks: the classic Einstein protocol [3] and the Eddington slow transportation method [4]. Both methods have certain limitations and difficulties in high accuracy nonlocal synchronization in which relativistic effects, such as the rotating disk problem, have to be taken into consideration. Einstein protocol is a two-way method, hence, it requires (1) an accurate knowledge of the one-way speed of light, that until now has not been measured conclusively on rotating reference systems and (2) the light propagation path to be the same in each direction. The Eddington transportation method relies on the physical movement of a clock, therefore,

this method is not practical for space applications. Recently, the nonlocal characteristics of entangled states have brought attention for possible protocols of high resolution clock synchronization [5] [6] [7].

In this letter we wish to report an experimental proof-of-principle demonstration of a new concept, based on the nonlocal feature of entangled states, that can be practically implemented for certain metrology applications such as high-accuracy one-way synchronization of clocks and high-accuracy positioning.

Our method relies on the measurement of the second order correlation function of entangled states. In particular, we consider the entangled photon pairs produced in a continuous wave (CW) pumped spontaneous parametric down conversion (SPDC) [8]. Very roughly speaking, the process of SPDC involves sending a pump laser beam into a nonlinear material, such as a non-centrosymmetric crystal. Occasionally, the nonlinear interaction inside the crystal leads to the annihilation of a high frequency pump photon and the creation of two lower frequency photons named as signal and idler. The creation time of either signal photon or idler photon is unknown; however, if the signal photon is registered at a certain time, the detection time of the idler photon can only happen at an unique precise time. In the reported experiment, both the signal photon and the idler photon are in the form of continuous wave, i.e.,  $\Delta t = \infty$ , nevertheless the time correlation measurement of the signal-idler at distance of  $3km$  has shown uncertainty in the order of picosecond.

According to quantum field theory, the probability of having a joint photo-detection event at space-time points  $(\mathbf{r}_1, t_1)$  and  $(\mathbf{r}_2, t_2)$  is proportional to the second-order correlation function of the fields [9]

$$G^{(2)}(\mathbf{r}_1, t_1; \mathbf{r}_2, t_2) = \langle E^{(-)}(\mathbf{r}_1, t_1)E^{(-)}(\mathbf{r}_2, t_2)E^{(+)}(\mathbf{r}_2, t_2)E^{(+)}(\mathbf{r}_1, t_1) \rangle \quad (1)$$

where  $E^{(-)}$  and  $E^{(+)}$  are the negative-frequency and the positive-frequency field operators of the detection events at space-time points  $(\mathbf{r}_1, t_1)$  and  $(\mathbf{r}_2, t_2)$ . For the two-photon entangled state of SPDC,  $G^{(2)}(\mathbf{r}_1, t_1; \mathbf{r}_2, t_2)$  can be written as the modulus square of a two-photon effective wavefunction, or biphoton:

$$G^{(2)}(\mathbf{r}_1, t_1; \mathbf{r}_2, t_2) = |\langle 0 | E^{(+)}(\mathbf{r}_2, t_2) E^{(+)}(\mathbf{r}_1, t_1) | \Psi \rangle|^2 \equiv |\Psi(\mathbf{r}_1, t_1; \mathbf{r}_2, t_2)|^2 \quad (2)$$

where  $|0\rangle$  stands for the vacuum, and  $|\Psi\rangle$  is the state of the signal-idler photon pair [10].

The two-photon effective wavefunction is calculated to be:

$$\Psi(r_1, t_1; r_2, t_2) = e^{-i(\omega_s^0 \tau_1 + \omega_i^0 \tau_2)} \mathcal{F}_{\tau_1 - \tau_2} \{f(\Omega)\} \quad (3)$$

where  $\mathcal{F}_{\tau_1 - \tau_2} \{f(\Omega)\}$  is the Fourier transform of the spectrum amplitude function  $f(\Omega)$ ,  $\tau_j = t_j - r_j/u_j$ ,  $j = 1, 2$ , and  $u_j$  is the group velocity at frequencies  $\omega_s^0$  and  $\omega_i^0$  along the optical paths 1 and 2, respectively.  $\omega_s^0$  and  $\omega_i^0$  are the central frequencies of the signal-idler radiation field.

The  $G^{(2)}(r_1, t_1; r_2, t_2)$  function for the two-photon entangled state of SPDC is thus

$$G^{(2)}(r_1, t_1; r_2, t_2) = |\mathcal{F}_{\tau_1 - \tau_2} \{f(\Omega)\}|^2. \quad (4)$$

This function, depending on  $\tau_1 - \tau_2$  is independent of the chosen reference coordinates: it is a Lorentzian invariant [11]. The spectrum amplitude function of the SPDC,  $f(\Omega)$ , provides all the information about the spectrum and the correlation properties of the signal-idler pair and it has been well studied [8] [12]. In the collinear case, for type-II and nondegenerate type-I SPDC, the spectral function is calculated as  $f(\Omega) \sim \text{sinc}(DL\Omega/2)$ , where  $L$  is the length of the crystal and  $D = \frac{1}{u_s} - \frac{1}{u_i}$  is the inverse group velocity difference for the signal and idler. For an 8mm LBO crystal pumped at 458nm (type-II), the estimated width of  $G^{(2)}(t_1 - t_2)$  is about 800 femtoseconds. For collinear degenerate type-I SPDC, the spectral function is  $f(\Omega) \sim \text{sinc}(D''L\Omega^2/2)$ , where  $D''$  is the second derivative of the dispersion function of the nonlinear material. In this case, the width of  $G^{(2)}(t_1 - t_2)$  is about 30 femtoseconds for the same size LBO crystal. Typical values for the natural width of  $G^{(2)}$  for SPDC are, then, on the order of a few femtoseconds to hundreds of femtoseconds. If  $r_1$  and  $r_2$  are well controlled, the measurement of  $t_1 - t_2$  can reach, in principle, the same order of resolution, making SPDC particularly suitable for implementing protocols for timing and positioning measurements with ultra high accuracy.

For example, consider a new protocol for one-way synchronization of two distant clocks: we have clock-1 in a space station and clock-2 in the laboratory (Fig. 1). The signal and idler photons are sent to two photon counting detectors  $D_1$  (in space) and  $D_2$  (on the ground). The photon registration times of the detectors,  $t_1$  and  $t_2$ , are recorded by two “event timers” whose time bases are provided by clock-1 and clock-2, respectively [13]. The individual time history records can be brought together through a classical communication channel for comparison. If the two clocks are synchronized, the joint detection of the signal-idler pair obtained by matching the photon registration time records will show maximum “coincidences”. If the clocks lose their synchronization, one has to rematch the records to achieve maximum coincidences by shifting one of them by a certain amount, that corresponds to how much the two clocks have lost their synchronization. The clocks can be adjusted and kept synchronized accordingly.

The initial synchronization of the two clocks is made in the following way: first we send the signal (with wavelength  $\lambda_s$ ) to detector  $D_1$  and the idler (with wavelength  $\lambda_i$ ) to detector  $D_2$ . The registration time difference,  $t_1 - t_2$ , at  $D_1$  and  $D_2$  is estimated:

$$t_1 - t_2 = \frac{r_1}{u_s} + t_0 - \frac{r_2}{u_i} \quad (5)$$

where  $t_0$  is the time offset of the two non-synchronized clocks. Then, we switch the signal and the idler, sending the idler to  $D_1$  and the signal to  $D_2$ . The registration time difference,  $t'_1 - t'_2$  of  $D_1$  and  $D_2$  will now be

$$t'_1 - t'_2 = \frac{r_1}{u_i} + t_0 - \frac{r_2}{u_s}. \quad (6)$$

Subtracting the two registration time differences, we have

$$\Delta t_- = (t_1 - t_2) - (t'_1 - t'_2) = D(r_1 + r_2) \quad (7)$$

where  $D = \frac{1}{u_s} - \frac{1}{u_i}$ .  $\Delta t_-$  is obtained from direct measurements and we assumed that  $r_2$  is known ( $D_2$  is in the laboratory). In some cases  $D$  is known or independently measurable, therefore the distance between the space station and the laboratory,  $r_1$ , is predictable

through the measurements of  $\Delta t_-$ . In other cases,  $r_1$  may be given or independently measurable, so, the value of  $D$  can be calibrated in the above procedure with ultra-high accuracy. In both cases substituting into either Eq. (5) or Eq. (6), the time offset  $t_0$  is thus estimated with the same order of accuracy as the measurement of  $t_1 - t_2$  and the clocks are synchronized accordingly. Notice that the measurement can be easily repeated for different values of  $r_2$ , so, for example, even in the case in which both  $D$  and  $r_1$  are unknown, measurements of  $\Delta t_-$  with different known values of  $r_2$  allow the evaluation of  $D$  and  $r_1$  simultaneously.

We performed the proof-of-principle experimental demonstration in the case in which  $r_1$  and  $r_2$  were known: in the laboratory, long optical fibers of known lengths were used to simulate the nonlocal condition. The setup is shown in Fig. 2. A single frequency  $Ar^+$  laser line of  $457.9nm$  was used to pump an  $8mm$  LBO crystal for type-II SPDC. The signal-idler radiations (centered at  $\sim 901nm$  and at  $\sim 931nm$  respectively) were separated from the pump laser beam by using filtering devices. The orthogonally polarized signal-idler pair was split by means of a polarizing beam splitter. Before the beam splitter, a half-wave plate was placed in order to perform the two measurements described previously: when the waveplate is at zero degrees, the signal is transmitted to  $D_1$  and the idler reflected to  $D_2$ ; when the waveplate is at 45 degrees, the idler is transmitted to  $D_1$  and the signal is reflected to  $D_2$ . In both measurements, the signal and idler radiation were fed into two  $1.5km$  long commercial optical fibers optimized for single-mode operation at  $1300nm$ . The signal-idler pair was then detected by two single-photon counting detectors. After a large number of signal-idler pair measurements, a histogram of the number of counts against  $t_1 - t_2$  (the resolution of the fast-timing electronics is  $3ps$ ) can be obtained. This distribution function corresponds to the  $G^{(2)}(t_1 - t_2)$  function previously described [14].

Fig. 3 shows the experimental results. The distribution function on the left corresponds to the case of signal- $D_1$  and idler- $D_2$  (half-wave plate at 0 degree) while the distribution function on the right corresponds to the case of idler- $D_1$  and signal- $D_2$  (half-wave plate at 45 degree). The presence of multiple peaks on each individual distribution function is a consequence of intermodal dispersion in optical fibers, which is a known effect in fiber optics

[16].

The calculated width of the effective two-photon wavefunction from a  $8mm$  type-II LBO SPDC, without the long optical fibers, is about  $800fs$ . The measured width of  $G^{(2)}(t_1 - t_2)$ , with the fibers, is around  $750ps$ . There are two contributions for the broadening of the  $G^{(2)}$  function: (1) dispersion in the optical fiber, which may be compensated nonlocally [15] [12] (the compensation is not included in this proof-of-principle experiment); (2) the time jitter of the photo-detector. The behavior of the biphoton in dispersive medium has been previously studied [12]. Using two fibers of  $1.5km$  length, the far-field zone condition is satisfied. Therefore, we expect  $G^{(2)}(t_1 - t_2)$  to take the shape of the spectrum function of the type-II SPDC  $|f(\Omega)|^2$  with a FWHM of  $600ps$ . Fig. 4 shows the central peak of the experimental data (for the case of half-wave plate at 45 degrees) compared with the theoretical expectation when the broadening contributions of (1) and (2) are taken into consideration. The fitting parameters  $k_s''$  and  $k_i''$  of the signal-idler radiations,  $2.76 \times 10^{-28} s^2/cm$  and  $2.96 \times 10^{-28} s^2/cm$ , respectively, are in agreement with the values specified by the manufacturer of the optical fiber.

By measuring the displacement of the central peak when the half-wave plate is rotated from 0 to 45 degrees ( $\Delta t_- = 5432 \pm 1ps$ ), and knowing the length of the fibers, the experimental value for  $D$ , using Eq. (7), was found to be  $1799.9 \pm 0.4ps/km$ , in agreement with the parameters of the fibers. Substituting the estimated value of  $D$  into either Eq. (5) or Eq. (6), the time offset is measured to be  $t_0 = 40369 \pm 1ps$ , which has the same order of accuracy of the  $t_1 - t_2$  measurement.

In conclusion, we successfully performed a high accuracy (picosecond) proof-of-principle experiment on distant clock synchronization ( $3km$ ). Besides the implementation of the novel one-way clock synchronization protocol, this experiment has also demonstrated a novel concept of quantum metrology for high accuracy nonlocal timing and positioning.

The authors thank M.H. Rubin, M. D'Angelo and D. Hudson for helpful discussions; G. Carter and H. Jiao for the loan of the fibers. This work was supported, in part, by NASA-CASPR program, NSF, and ONR.

## REFERENCES

- [1] T. B. Bahder, "Clock Synchronization and Navigation in the Vicinity of the Earth", gr-qc/0405001.
- [2] W. Wayt Gibbs, Scientific American, Special issue, September 2002.
- [3] A. Einstein, Ann. Phys., **17**, 891 (1905).
- [4] A. S. Eddington, "The Mathematical Theory of Relativity", Chelsea Publishing Company, New York, (1924)
- [5] Richard Jozsa, Daniel S. Abrams, Jonathan P. Dowling, and Colin P. Williams. Phys. Rev. Lett. **85**, 2010 (2000).
- [6] Vittorio Giovannetti, Seth Lloyd and Lorenzo Maccone, Nature. **412**, 417 (2001).
- [7] V. Giovannetti, S.Lloyd, L.Maccone, and F.N.C.Wong, Phys. Rev. Lett. **87**, 117902 (2001).
- [8] D.N. Klyshko, *Photons and Nonlinear Optics* (Gordon & Breach, New York,1988).
- [9] R.J. Glauber, Phys. Rev. **130**, 2529 (1963); **131**, 2766 (1963).
- [10] M.H. Rubin, D.N. Klyshko, Y.H. Shih, and A.V. Sergienko, Phys. Rev. A **50**, 5122 (1994).
- [11] Thomas B. Bahder, Phys. Rev.D **68**, 063005 (2003).
- [12] A.Valencia, M.V.Chekhova, A.Trifonov and Y.Shih, Phys. Rev. Lett. **88**, 183601 (2002).
- [13] C. Steggerda *et al*, Proceedings of the 10th International Workshop on Laser Ranging Instrumentation, Ed. F.M. Yang, Chinese Academy of Sciences Press, 404 (1996).
- [14] L. Mandel and E. Wolf, *Optical Coherence and Quantum Optics*(Cambridge University Press, 1995).
- [15] J.D. Franson, Phys. Rev. A, 45, 3126 (1992).

- [16] The fibers are optimized for single mode operation at  $1300nm$ . For the operating wavelengths (approximately 901 nm and 931 nm) two modes are excited [17]. These modes have different group velocities that result in different time delays and causing the side peaks.
- [17] John M. Senior, *Optical Fiber Communications Principles and Practice* (Prentice Hall International, 1992).



## FIGURES

FIG. 1. Schematic setup of a novel protocol for one-way distant clock synchronization.

FIG. 2. Schematic setup of the proof-of-principle experiment.

FIG. 3. A typical histogram, the number of counts vs detection time difference  $t_1 - t_2$ . Curve on the left: half-wave plate at 0 degrees; Curve on the right: half-wave plate at 45 degrees. The presence of side-peaks is due to the excitation of side-modes in the fiber.

FIG. 4. Central peak of the measured distribution function of  $t_1 - t_2$ . The solid line is a theoretical fitting curve of  $G^{(2)}$  considering the broadening contributions of the propagation dispersion and the jitter of the photon counting detectors.

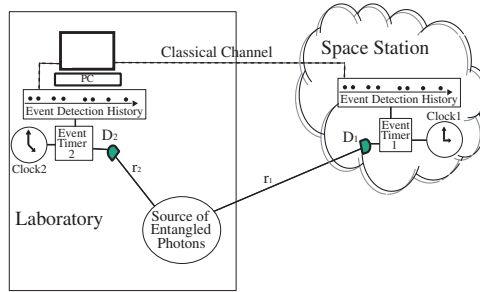


Fig. 1: Alejandra Valencia, Giuliano Scarcelli, Yanhua Shih

Figure 1. Alejandra Valencia, Giuliano Scarcelli, and Yanhua Shih.

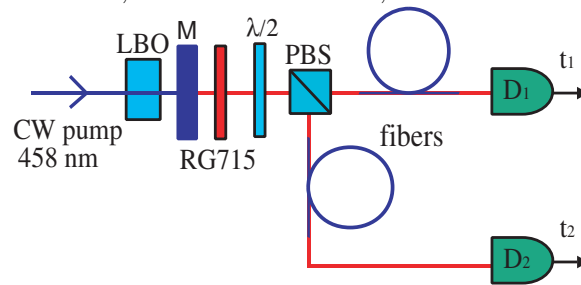


Figure 2. Alejandra Valencia, Giuliano Scarcelli, and Yanhua Shih.

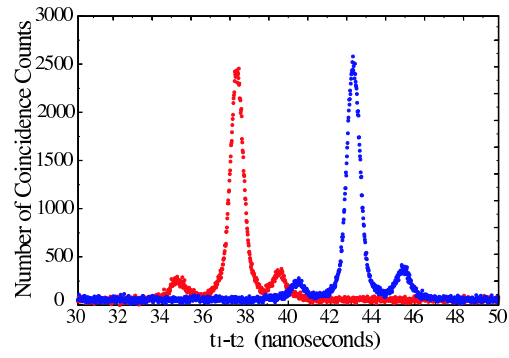


Figure 3. Alejandra Valencia, Giuliano Scarcelli, and Yanhua Shih.

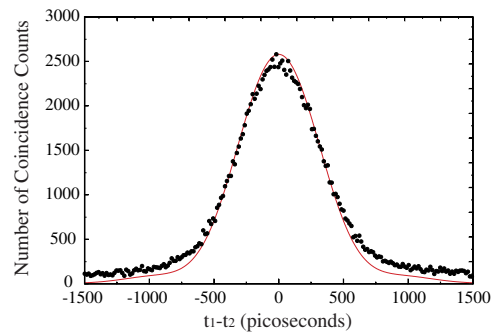


Figure 4. Alejandra Valencia, Giuliano Scarcelli, and Yanhua Shih.